Journal of Cerebral Blood Flow & Metabolism (2015) 35, 213–220

www.jcbfm.com

ORIGINAL ARTICLE

Assessing cerebrovascular reactivity abnormality by comparison to a reference atlas

Olivia Sobczyk[1], Anne Battisti-Charbonney[2], Julien Poublanc[2], Adrian P Crawley[2], Kevin Sam[2,3], Jorn Fierstra[4], Daniel M Mandell[2], David J Mikulis[1,2], James Duffin[3,5] and Joseph A Fisher[1,3,5]

Attribution of vascular pathophysiology to reductions in cerebrovascular reactivity (CVR) is confounded by subjective assessment and the normal variation between anatomic regions. This study aimed to develop an objective scoring assessment of abnormality. CVR was measured as the ratio of the blood-oxygen-level-dependent magnetic resonance signal response divided by an increase in CO_2, standardized to eliminate variability. A reference normal atlas was generated by coregistering the CVR maps from 46 healthy subjects into a standard space and calculating the mean and standard deviation (s.d.) of CVR for each voxel. Example CVR studies from 10 patients with cerebral vasculopathy were assessed for abnormality, by normalizing each patient's CVR to the same standard space as the atlas, and assigning a *z*-score to each voxel relative to the mean and s.d. of the corresponding atlas voxel. *Z*-scores were color coded and superimposed on their anatomic scans to form CVR *z*-maps. We found the CVR *z*-maps provided an objective evaluation of abnormality, enhancing our appreciation of the extent and distribution of pathophysiology compared with CVR maps alone. We concluded that CVR *z*-maps provide an objective, improved form of evaluation for comparisons of voxel-specific CVR between subjects, and across tests sites.

Journal of Cerebral Blood Flow & Metabolism (2015) **35,** 213–220; doi:10.1038/jcbfm.2014.184; published online 12 November 2014

Keywords: carbon dioxide; cerebrovascular reactivity; humans; oxygen

INTRODUCTION

Cerebrovascular Reactivity

The measurement of cerebrovascular reactivity (CVR), whereby a strong vasoactive stimulus is applied to expose occult clinical limitations in regional cerebral blood flow (CBF) reactivity,[1] constitutes a cerebrovascular stress test. Quantitatively, CVR is defined as the change in CBF in response to a measurable stimulus. A surrogate high-resolution measure of changes in CBF can be obtained by exploiting the blood-oxygen-level-dependent (BOLD) effect of magnetic resonance imaging (MRI). A measurable increase in the end-tidal partial pressure of CO_2 ($P_{ET}CO_2$) can be used as a surrogate measure for the true independent stimulus, the partial pressure of CO_2 in arterial blood ($PaCO_2$). Cerebrovascular reactivity is then defined as the percentage of change in BOLD signal per mm Hg change in $PaCO_2$. Cerebrovascular reactivity values can be color coded and superimposed, on the corresponding voxel on an anatomic scan to generate CVR maps.[2]

Clinical Aspects of Cerebrovascular Reactivity Maps

Of particular interest in the CVR maps are areas of paradoxical reductions in flow after the application of a vasodilatory stimulus, termed as 'steal'. Steal has been shown to exist in deep white matter in healthy people,[3] in CVR maps of patients with steno-occlusive vascular disease,[4] and with pathologic conditions including arteriovenous malformations[5] and vasculitis.[6] Steal physiology is associated with cortical thinning,[2] white matter microangiopathic disease,[7] cognitive decline,[8,9] and enhanced risk of stroke.[10,11]

Detecting Vascular Pathophysiology with Cerebrovascular Reactivity Maps

Whereas the presence of steal is highly specific for identifying compromised CVR, the absence of steal does not necessarily imply normal CVR. For example, CVR may be considerably reduced, but steal is absent if the stimulated demand fails to exceed its supply capacity. Alternatively, if the reduction of CVR is widespread and uniform, rather than localized, a differential in vasodilatory capacity between vascular territories may not exist and therefore, steal may not occur.[1] Steal may also not occur if compromised vessels maintain some vasodilatory reserve. Under these conditions, the absolute value of CVR may be less than 'normal' but the extent of reduction cannot be assessed unless the normal range of CVR is known for each anatomic location.

The range of CVR across healthy subjects is large because of factors such as age[12] and gender,[13] and varies within subjects from region to region. Thus, even substantial reductions in CVR in one region will overlap with normal values in another, making it challenging to distinguish reduced CVR because of pathophysiology from normally low CVR. Because the interpretation and assessment of CVR maps currently relies on subjective assessments, it is difficult to identify reduced CVR short of that causing 'steal'.

[1]Institute of Medical Science, University of Toronto, Toronto, Ontario, Canada; [2]Joint Department of Medical Imaging and the Functional Neuroimaging Laboratory, University Health Network, Toronto, Ontario, Canada; [3]Department of Physiology, University of Toronto, Toronto, Ontario, Canada; [4]Department of Neurosurgery, University Hospital Zurich, Zurich, Switzerland and [5]Department of Anaesthesia and Pain Management University Health Network, University of Toronto, Toronto, Ontario, Canada. Correspondence: O Sobczyk, Institute of Medical Science, University of Toronto, Medical Sciences Building, 1 King's College Circle, Toronto, Ontario, Canada M5S 1A8.
E-mail: o.pucci@mail.utoronto.ca
Received 9 August 2014; accepted 25 September 2014; published online 12 November 2014

Aim of the Study

The aim of this study was to enhance the interpretation of CVR maps by applying an objective scoring system for CVR by statistical comparison to a reference cohort of healthy individuals. To show the effectiveness of the scoring system we examined the CVR of 10 patients with known cerebrovascular disease.

MATERIALS AND METHODS

Subjects and Ethical Approval

These studies conformed to the standards set by the latest revision of the Declaration of Helsinki. All studies were approved by the Research Ethics Board of the University Health Network and all subjects gave written informed consent. We recruited 46 healthy volunteers for the creation of the reference CVR atlas by advertisement and word of mouth. This cohort consisted of subjects of both sexes and any age who claimed to be in good health, denied a history of neurologic disease, were nonsmokers, and were taking no medication. They were asked not to engage in heavy exercise or drink caffeinated drinks on the day of the scan. The characteristics of these subjects are presented in Table 1. We then drew examples from 10 patients in our database of the research ethics board-approved CVR studies in patients with known symptomatic cerebrovascular disease.[14] They were selected without regard for age, sex, diagnosis, or findings on vascular imaging or CVR studies. All 10 patients were chosen and grouped before any of their data was analyzed. None were rejected after analysis.

Experimental Protocol

Hypercapnic Stimulus. The implementation of prospective end-tidal gas control has been described in detail elsewhere.[15] In brief, subjects were fitted with a face mask, and connected to a sequential gas delivery breathing circuit.[16] The patterns of $P_{ET}CO_2$ and $P_{ET}O_2$ were programmed into the automated gas blender (RespirAct™, Thornhill Research, Toronto, Canada) running the prospective gas targeting algorithm of Slessarev *et al*.[17] A standardized step CO_2 stimulus was implemented, consisting of the following sequence: a baseline $P_{ET}CO_2$ of 40 mm Hg for 60 seconds, step to a hypercapnia of 50 mm Hg for 45 seconds, baseline for 90 seconds, hypercapnia for 120 seconds, and return to baseline for 60 seconds, all during isoxic normoxia targeted at 100 mm Hg.

We chose a nonperiodic stimulus function so that a steal effect (reversed sign amplitude) would not be confused with a simple delay in response close to half the period of a periodic function. However, the exact characteristics of the stimulus is unimportant as long as the independent variable ($PaCO_2$) is known, is repeatable with high fidelity, and is the same between patients and atlas subjects.

We chose a fixed baseline PCO_2 of 40 mm Hg because this resting value is found in most subjects. In some subjects this PCO_2 will be higher than their resting PCO_2 and affect their CVR measures,[1] but the same conditions apply to the atlas subjects and therefore will be accounted for when assessing the normal range of CVR. For the healthy and patient cohorts the mean and standard deviation (s.d.) change in $P_{ET}CO_2$ was 9.2 (0.7) mm Hg and 9.0 (0.8) mm Hg, respectively. This methodology has been shown to control the CO_2 stimulus such that $P_{ET}CO_2$ is equivalent to $PaCO_2$.[18,19]

Table 1. Demographic of healthy subject atlas

	Number
Age range	
20 to 30	24
30 to 40	10
40 to 50	5
50 to 60	2
60 to 70	3
70+	2
Sex	
F	16
M	30

F, female; M, male.

Magnetic Resonance Imaging Protocol for Cerebrovascular Reactivity Map generation. Magnetic resonance imaging was performed with a 3.0-Tesla HDx scanner using an eight-channel phased-array receiver coil (Signa; GE Healthcare, Milwaukee, Wisconsin), and consisted of BOLD acquisitions with echo planar imaging gradient echo (TR/TE = 2000/30 ms, field of view 24 × 24 cm, matrix size 64 × 64, number of frames = 254, 39 slices, slice thickness 5 mm, and flip angle = 85°). The acquired MRI and $P_{ET}CO_2$ data were analyzed using AFNI software (National Institutes of Health, Bethesda, Maryland; http://afni.nimh.nih.gov/afni).[20] BOLD images were first volume registered and slice-time corrected and coregistered to an axial three-dimensional T1-weighted inversion recovery prepared fast-spoiled gradient echo volume (TI/TR/TE = 450/8/3 ms, matrix size 256 × 256, field of view 22 × 22 cm, slice thickness = 1 mm, and flip angle = 15°) that was acquired at the same time.[21] $P_{ET}CO_2$ data was then time-shifted to the point of maximum correlation with the whole brain average BOLD signal. A linear, least-squares fit of the BOLD signal data series to the $P_{ET}CO_2$ data series (i.e., CVR) was then performed on a voxel-by-voxel basis, together with a linear trend regressor. For displaying CVR maps, voxels with a correlation coefficient between −0.25 and +0.25 were eliminated before color-coding the remaining CVR values (see spectrum in Figure 3). This method has been described in greater detail elsewhere.[2]

Analysis of Cerebrovascular Reactivity Maps

Constructing the Magnetic Resonance Imaging Cerebrovascular Reactivity Atlas. Analytical processing software (SPM8; Wellcome Department of Imaging Neuroscience, University College, London, UK; http://www.fil.ion.ucl.ac.uk/spm/software/spm8), was used to coregister each of the individual T1-weighted fast-spoiled gradient echo brain volumes from the healthy cohort into MNI (Montreal Neurological Institute) standard space, as defined by a T1-weighted MNI152 standard template[22] using a 12-parameter [23] affine transformation followed by nonlinear deformations. The calculated transformation for each individual was then applied to the BOLD data.

A spatial smoothing of full-width half-maximum 5 mm was applied to each voxel. Assumption for normality was tested using the Anderson–Darling test (the statistical test for normality provided in AFNI (National Institutes of Health)) with P values >0.05 assumed to pass the test. As most voxels (60%) did pass this threshold, and these were diffusely distributed throughout the brain, the simplifying assumption was made that the CVR for each voxel was normally distributed. The mean (μ) and associated standard deviation (σ) of CVR for each voxel was calculated (AFNI software (National Institutes of Health)[20]). Maps were then constructed for μ and coefficient of variation (σ/μ) to characterize the atlas.

Cerebrovascular Reactivity z-map generation. The generation of an individual's CVR *z*-map consisted of three steps. First, a spatial normalization of the individual's anatomic scan and CVR map[22] using a MNI152 SPM distributed template was produced. Second, the CVR of each voxel (x) was scored in terms of a *z*-value (i.e., $z = (x\text{-}\mu)/\sigma$;[24]). Finally, a color was assigned to each *z*-score (see scale in Figure 3) to indicate the direction and magnitude (in z-values) of the differences from the mean of the corresponding atlas voxel. CVR and CVR *z*-scores were superimposed on the corresponding anatomic scans to allow comparison of the CVR and its *z*-score. Note that CVR voxels that are positive but lower than the atlas mean for that voxel will have negative *z*-scores. Greater specificity for identifying underlying vascular pathophysiology was assumed to be connoted by greater absolute value of *z*-scores and the confluence of similarly scored voxels in both CVR and CVR *z*-maps (Figures 4 and 5).

RESULTS

Normal Cohort Cerebrovascular Reactivity Characteristics

Figure 1 shows maps of the mean CVR and coefficient of variation of the reference atlas. It illustrates the large and complex pattern of regional variability that remains after deliberate smoothing and the effects of misregistration and partial voluming. These color patterns represent the voxel means from which the *z*-maps are calculated.

The spatial distribution of the results of the Anderson–Darling statistical test of normality applied to the 46 healthy subjects CVRs

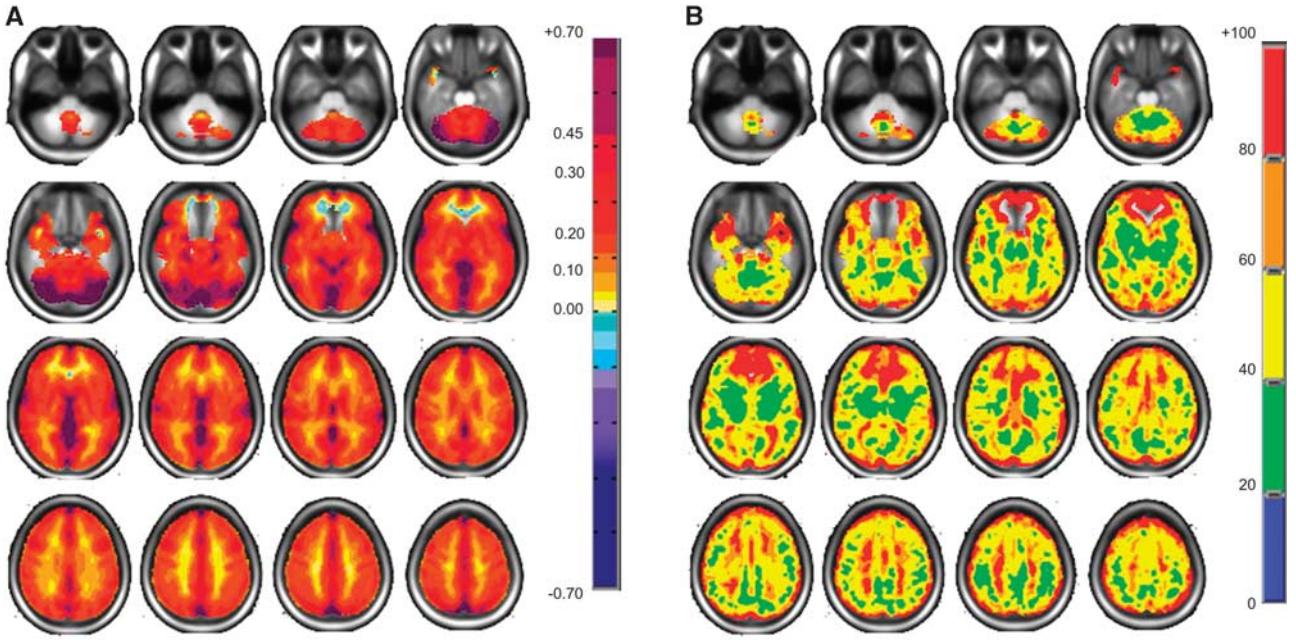

Figure 1. Axial slices for the normal cohort atlas displaying spatial distributions. (**A**) Mean CVR values colored according to the scale shown on the right in percentage of BOLD change per mm Hg $P_{ET}CO_2$ change. (**B**) Coefficient of variation values with color scale on right in percentage. BOLD, blood oxygen level-dependent; CVR, cerebrovascular reactivity; $P_{ET}CO_2$, end-tidal partial pressure of CO_2.

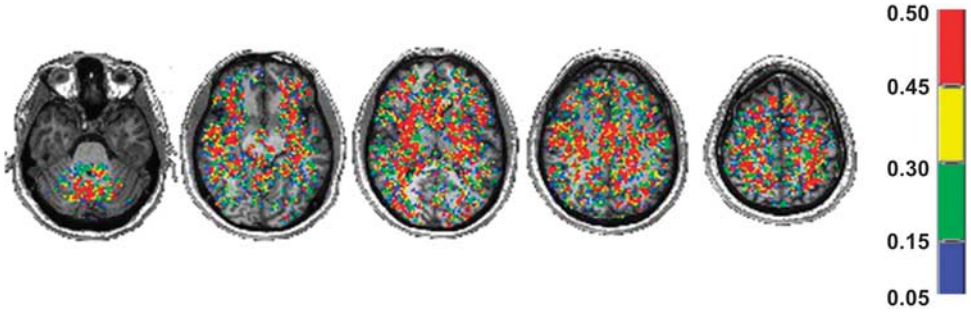

Figure 2. Axial slices displaying the spatial *P* value results of the Anderson–Darling normality test. All voxels shown were found to have a *P* value >0.05.

graphed into the MNI standard brain is shown in Figure 2. At least 60% of the voxels had a *P* value >0.05; these voxels were fairly evenly distributed throughout the brain.

Z-Map Examples

For comparison purposes, we present the CVR and its accompanying *z*-map from a healthy subject not included in the atlas in Figure 3. This method is known as the 'jackknife' procedure and is used when taking a subject from a reference atlas and comparing them back to the atlas to perform *z*-scoring.[24] The *z*-maps of the 10 patients drawn from our database are shown in Figures 4 and 5, and descriptions related to each patient are presented Table 2.

DISCUSSION

Main Findings

The main outcomes of this study are, first, the generation of an atlas of the normal distribution of MRI BOLD-generated CVR in 46 healthy subjects. Second, the application of this reference atlas to statistically score MRI BOLD-based CVR maps in a case series of patients with symptomatic neurovascular disease; controlling the CVR for anatomic location, and scanner-specific technical and acquisition sequence idiosyncrasies. The *z*-scores added information regarding the spatial distribution and severity of the CVR deficits, and occasionally even detected their presence. Such changes in BOLD signal may be related back to the underlying pathophysiology.[1]

Optimizing *z*-Maps

Previously, *z*-maps examined to what extent a steady state condition deviated from normal. The subject-to-subject, and test-to-test variability in the reference atlas was minimized by standardizing the measurement parameters and conforming all scans to a standard space.[25,26] In our study, it was necessary to minimize the variation in the stimulus by using an MRI compatible method that applied a consistently repeatable stimulus. Whereas breath-holding and inhalation of carbogen (5% CO_2 in oxygen) are inexpensive, simple, and MRI compatible, they do not reliably

result in consistent end-tidal[27,28] or arterial values[29] (see, ref. 13 for discussion), which are the true independent variables affecting CBF. We minimized the variation in the stimulus by using a prospective end-tidal targeting method. This method accurately targets $P_{ET}CO_2$, but more importantly, $PaCO_2$.[18,19,30]

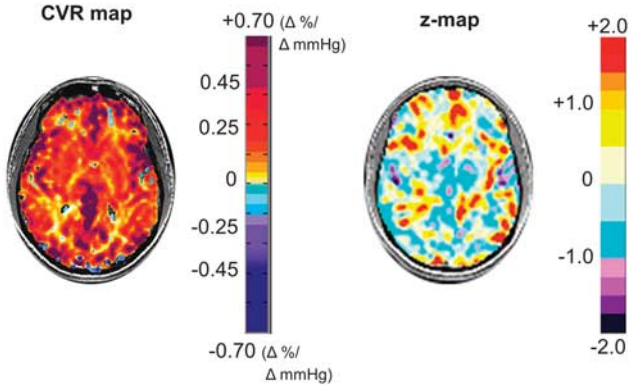

Figure 3. An axial slice from a healthy subject's CVR map is shown on the left displaying the spatial distribution of CVR values colored according to the scale shown on the right in percentage of BOLD change per mm Hg $P_{ET}CO_2$ change. The corresponding CVR *z*-map and its color scale are shown on the right. The CVR *z*-map provides a perspective on the (statistical) normality of CVR in the CVR map. This figure illustrates the extent of expected high statistical abnormality, as a result of physiologic, technical (both experimental and analytical), and anatomic variation in the subject as well as errors in the matching of voxels during coregistration. BOLD, blood oxygen level-dependent; CVR, cerebrovascular reactivity; $P_{ET}CO_2$, end-tidal partial pressure of CO_2.

A further issue to consider with the *z*-map approach is whether to use a threshold *z*-value to isolate abnormal voxels. Prevailing practice for CVR maps is the division into positive and negative (i.e., steal and nonsteal) territories.[2,8] Other studies comparing subjects to reference atlases apply thresholds of 1.5,[31] 2,[32,33] and even 3[34] to the z-values to mark 'abnormal' voxels in their maps. However, our view is that such thresholding is disadvantageous because it reduces the sensitivity for detecting abnormal voxels.

To illustrate this point, consider the following situation. In a *z*-map of a normal subject, the average *z*-value of any region of interest (ROI) should be 0, with the individual z-values normally distributed ~0. Now consider a test subject whose average *z*-score for that particular ROI is, for example, 0.72. If this value is greater than 2 s.d. of the mean *z*-score for that ROI, then the CVR in that ROI, albeit small, must be classed as abnormal. However, thresholding individual voxel *z*-scores for 2, or even 1.5 would not detect such abnormalities. Indeed, the proper thresholds for z-values are not, as in previous studies, relative to the variance of the CVR, but to that of the *z*-scores themselves. These are the issues that indicate the way to set up receiver-operator characteristics calculations[24,35] for identifying vascular pathology affecting CVR. With these considerations in mind we eschewed thresholding the CVR *z*-maps.

Characteristics of the Reference Atlas

The CVR atlas represents the distribution of CVR and its variance in the human brain, as reflected by our sample. It incorporates the regional anatomic differences in the response of the BOLD signal resulting from (1) tissue factors, such as age, sex, O_2 consumption,

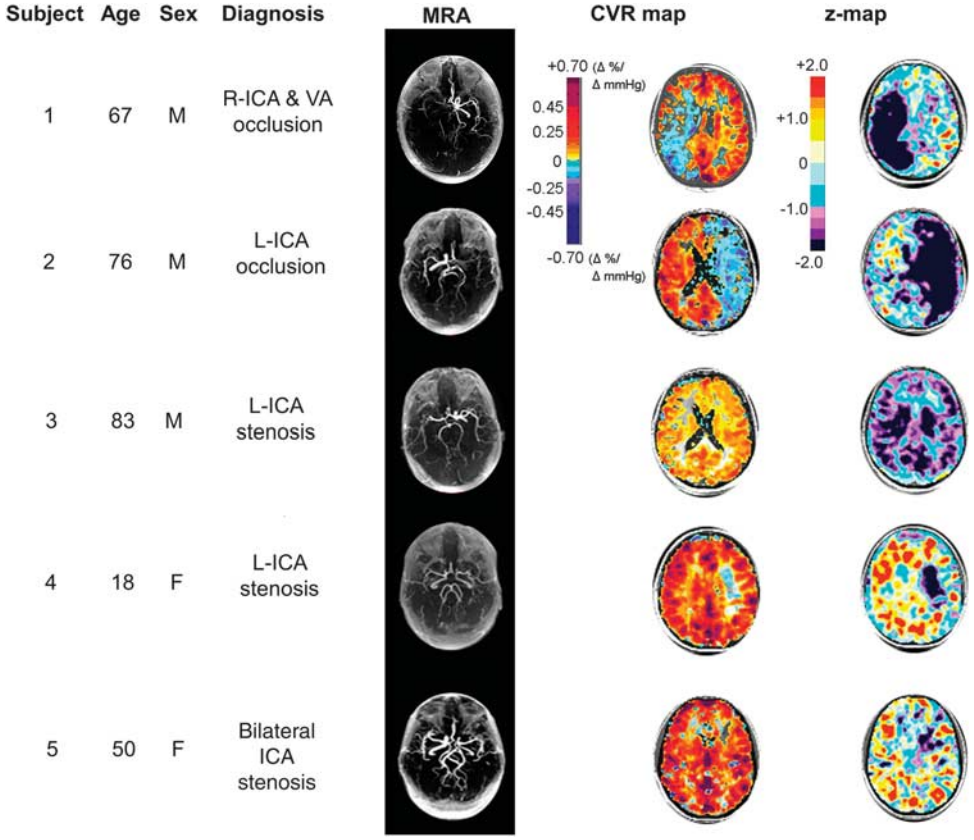

Figure 4. Example set of five patients with varying levels of large vessel cerebral vascular disease chosen from our database and then further analyzed by *z*-scoring the CVR map relative to a normal atlas. Table 2 provides additional information and commentary for each subject. CVR, cerebrovascular reactivity; ICA, internal carotid artery; L, left; MRA, magnetic resonance angiogram; R, right; VA, vertebral artery.

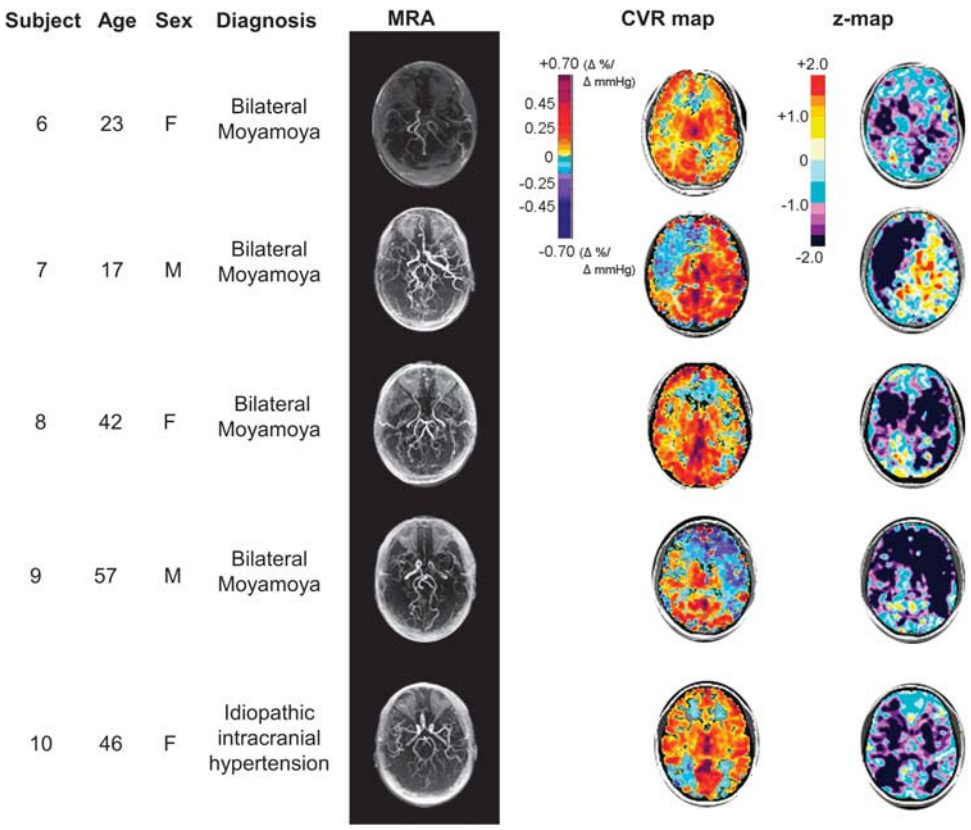

Figure 5. Example set of four patients with Moyamoya disease and one patient with idiopathic intracranial hypertension, chosen from our database and then further analyzed by *z*-scoring the CVR map relative to a normal atlas. Table 2 provides additional information and commentary for each subject. CVR, cerebrovascular reactivity; MRA, magnetic resonance angiogram.

capillary density, changes in blood volume, differences in blood arrival time, and vascular response time; (2) physiologic factors such as genetic makeup, variations in diet, sleep pattern, time of day, hormonal level, physical fitness, blood pressure and blood pressure response to hypercapnia, and state of mind; and (3) possible uncertainties in technical and mechanical changes in the MRI system over time. These form the background 'noise', from which a patient's abnormal voxels, their distribution, and the extent of their deviation, must be discerned.

In principle, controlling for sources of variability such as age, sex, medication, and presence of comorbidities in the reference atlas would tend to isolate the disease process as the dominant source of divergence of CVR; for example, matching age, sex, medication, and other physiologic features to the target study group (for example young men with multiple sclerosis), and reducing all technical and methodological sources of variability, would leave the disease process as the dominant source of divergence of CVR from that of the reference cohort.

Characteristics of the Patient Cohort

The examination of our patient data illustrates the value added to CVR interpretation by *z*-maps. Subjects 3, 6, 8, and 10, in Figures 4 and 5 illustrate the difficulty in confidently interpreting abnormal CVR in areas not showing steal. In patients 3 and 6, the reductions in CVR are symmetrical; there is little 'steal' as no territory has sufficiently greater vasodilatory reserve capacity over the other.[1] This mechanism can also explain the small negative CVR values despite profound reductions in CVR *z*-scores in subjects 8 and 10. In subjects 4 and 5, the robust CVR is likely because of the recruitment of collateral blood flow, and had been interpreted as 'normal' in the original studies. However, the *z*-map analysis now highlights a previously unrealized reduction in CVR in the left middle cerebral artery territory. A summary of the clinically relevant advantages *z*-maps provide beyond plain CVR maps is presented in Table 3.

One aspect of the *z*-maps of our patient cohort is that lesions appear to extend smoothly across tissue boundaries. Our scans were not segmented into white matter and gray matter, which have different CVR values. They are therefore susceptible to partial volume effects, which can be seen as a progression of CVR values at the interfaces between them and with cerebrospinal fluid. As a result there is a tendency for any abnormalities in CVR isolated to either side of the boundary is to overlap the other, although the magnitude of this effect is offset by the effect of blurring to increase the variability of CVR values (and reduce the sensitivity) on both sides of the boundary.

We also note that most of the patients presented with protean transient symptoms and were otherwise remarkably asymptomatic. Furthermore, the extent of the neurovascular changes provoked by the hypercapnic challenge and measured by the CVR and their *z*-maps are very much out of proportion to the clinical symptoms. This indicates the considerably greater sensitivity of neuroimaging, including CVR, in detecting occult neurovascular disease compared with clinical assessment.

Using *z*-Maps to Compare Cerebrovascular Reactivity Across Platforms

An early use of the *z*-map approach was to enable a voxel-by-voxel comparison of the degree of brain atrophy and brain metabolism by generating MRI and positron emission tomography atlases, respectively, and converting values generated from each scan to *z*-scores.[24,31] The *z*-scores relate to the mean and

Table 2. Clinical comments concerning Figures 4 and 5

Subject	*Detailed diagnosis*	*CVR map and z-map description*
1	Previous Hx of stroke. Presented with R TIAs. Angiography shows R ICA occlusion and VA stenosis	The CVR map shows steal in R MCA and PCA territories. The *z*-maps show not only the extent, but also the severity of abnormality. The lowest *z*-scores correspond to the 'blue' of the CVR; the *z*-map confirms that the CVR in the WM on the left side is also diffusely reduced
2	R TIA presentation. Angiography shows L ICA occlusion	The CVR map shows that steal is present in the entire left hemisphere. The *z*-maps indicate the severity of the abnormality and the extent of hemodynamic involvement. The CVR in the R hemisphere also appears reduced (Sam *et al.*[44])
3	TIA. L ICA stenosis	Despite the unilateral vascular lesion, the CVR map is symmetrical, but appears reduced. The *z*-maps confirm marked reduction in CVR throughout the cortex and deep WM regions
4	Hx previous stroke. L ICA stenosis	The CVR map appears to be normal except for a mild CVR impairment in the area of the stroke. The *z*-maps confirm that CVR is normal in the normal-appearing areas of the CVR map; severe reduction of CVR in area of stroke
5	Stroke in the watershed area extending into the MCA. Stroke in the left subcortical region. Left cavernous ICA occlusion and R ICA stenosis	The CVR map appears to be normal with some reduction in the left subcortical area. The *z*-maps confirmed the normality of much of the scan but show that the subtle-appearing changes of the CVR map are in fact severely abnormal
6	Hx astrocytoma of the optic chiasm as a child, Rx with surgical resection, chemotherapy, and radiotherapy. L EC-IC bypass 2 years ago for MM	The CVR map appears to be close to normal but gives an impression that CVR was somewhat diffusely reduced with little visible steal. The *z*-maps emphasize that there are widespread reductions in CVR and indicate their severity, particularly in the R WM region which was not apparent from the CVR. Note despite the severity of reductions in CVR, the necessary conditions to generate steal were not met (Sobczyk *et al.*[1])
7	Hx of repeat TIAs	The CVR map shows impaired CVR in the right MCA, which extends to the ACA territory, with the severity difficult to judge; CVR elsewhere appears normal. The *z*-maps scores the severity and extent of reduced CVR in the area of steal, but shows the extent of impaired CVR exceeds that of steal; confirms normal reactivity in the contralateral hemisphere on the side of the EC-IC bypass
8	Hx MM with intraventricular hemorrhage	The CVR map shows that CVR is reduced globally, with reduced CVR and possibly some steal evident on the left. The *z*-maps show that the bilateral CVR impairment in both R and L MCA territories is severe beyond 2 s.d.
9	Hx MM with infarct. Post-R EC-IC bypass; rescanned for assessment of continuing TIA	The CVR map indicates a persistent reduction of CVR throughout the R MCA region. The *z*-maps confirm these bilateral reductions in CVR, much worse in the areas of steal
10	Idiopathic intracranial hypertension	The CVR map shows areas of steal in the WM of the frontal and occipital lobes, with normal-appearing CVR in the rest of the brain. The *z*-maps, however, confirm bilateral severe reduction in CVR in deep GM and WM, that was not realized from an examination of the CVR map

ACA, anterior cerebral artery; CVR, cerebrovascular reactivity; EC-IC, external carotid to internal carotid; GM, gray matter; Hx, history; ICA, internal carotid artery; L, left; MCA, middle cerebral artery; MM, Moyamoya; PCA, posterior cerebral artery; R, right; Rx, treatment; s.d., standard deviation; TIA, transient ischemic attack; VA, vertebral artery; WM, white matter.

variance of a value in its reference atlas; not to the imaging method (positron emission tomography, single photon emission computed tomography, computerized tomography scan,[36] or MRI). They are also not related to the MRI scanner used, or the scanning sequence, as long as these are consistent across the subject and the reference cohort. With respect to CVR *z*-maps, the consistency of the stimulus, $PaCO_2$, which is independent of the ventilatory response,[17] is a crucial enabling element. For example, the $PaCO_2$ stimuli resulting from breath-holding and inspiring a fixed PCO_2 are patient dependent and thus highly variable,[15] and therefore unsuitable. With a consistent PCO_2 stimulus, CVR *z*-scores should enable the comparison of CVR scores between centers. However, despite a two-decade history of CVR studies and use of *z*-scoring, such comparisons have yet to be reported for CVR.

Nevertheless, at least initially, we suggest that it is safest to generate a unique atlas for each scanner, which involves the time and expense of obtaining ethics board approval, generating the data, and performing the analysis. Furthermore, the *z*-score approach locks in a sequence and methodology, which constrains adjustments by scanner operators to optimize scan quality. On the positive side, making a reference atlas can be seen as a onetime 'calibration'. Although pooling atlases from multiple scanners may address this issue, it would also increase the atlas variability and therefore reduce its sensitivity.

Table 3. Summary of comparison of CVR and its *z*-maps

	CVR	*z-map*
Sensitivity	Low: mainly identifies presence/absence of steal	Higher sensitivity by detecting graded reductions in CVR short of steal.
Specificity	High: steal is accepted sign of abnormal vasculature.	Lower specificity mitigated by (1) normalization of CVR to normal range for region highlights abnormal CVR and (2) confluence of reduced *z*-scores is statistically unlikely in tissue with normal CVR
Anatomic location specificity	No: CVR maps score absolute values of CVR	Yes: *z*-score normalizes CVR for anatomic location
Identification of abnormality distribution	Identifies only the distribution where steal occurs as abnormal	Identifies the distributions of various grades of reduced CVR beyond that of steal
Platform specificity	CVR can be performed on any magnet, however, CVR is specific for that magnet	Probably: each platform may require its own unique atlas
Comparison across platforms	Possibly: requires, at a minimum, standardized MR sequence parameters and uniform stimulus *across* platforms	Yes: requires only consistency of sequences and stimulus between atlas and patient within each platform: z-values should then be comparable across platforms

CVR, cerebrovascular reactivity; MR, magnetic resonance.

Limitations

We used BOLD as a surrogate for CBF, which has been accepted as valid for CBF during functional MRI measurements for a considerable time.[37] Flow sensitive alternating inversion recovery and BOLD MRI methods have been favorably compared with other surrogate measures of CBF such as positron emission tomography and arterial spin labeling, including comparisons in patients with steno-occlusive vascular disease.[38,39] Blood oxygen level-dependent has advantages over positron emission tomography, in that it is noninvasive, generally available, and less expensive. It has greater time and spatial resolution than arterial spin labeling, provides greater coverage, requires shorter scan times, and is a sequence more commonly available on clinical scanners. Specific artefacts associated with BOLD, such as those arising from differences in baseline metabolism, alterations in cerebral blood volume (such as increased signal changes over venous pools of blood), and hemoglobin concentration—all these artefacts contribute to the atlas variability and are therefore controlled by the *z*-map approach.

This atlas of 46 healthy subjects was not developed for a specific disease, age group or sex, and commensurate with this aspect, neither did we select our study cohort by these criteria. Thus, the atlas contains a wide range of ages, and we accepted the possible limitation in sensitivity for this study when studying a cohort of a narrower age range. If age is a large determinant of CVR, the extensive age range in the atlas will result in a reduction in sensitivity of the *z*-maps but will also result in greater specificity. In any event, there is no consensus to what extent age affects CVR. Indeed, using our atlas data we found no correlation of CVR with age (Pearson correlation coefficient = – 0.11), and others have made similar observations.[40,41] Similarly discrepancies in sex, comorbidities or other anthropomorphic factors between the study cohort and atlas will further reduce the sensitivity, and increase specificity.

Our atlas included about twice as many subjects as other *z*-score studies,[24,31] and so provided a more robust specificity for our *z*-maps. The *z*-scores illustrated that the CVR in each patient, at least in some region, was substantially distinct from that of any of the healthy subjects regardless of the sex and age distribution.[42] This suggests that the *z*-map analysis may also be used to identify abnormalities of CVR in a number of other neurologic diseases.

The example patients we chose were not intended to represent typical findings for any particular pathology, but to illustrate the range of images produced by *z*-score analysis relative to a reference atlas. We emphasize that our study also does not evaluate whether *z*-map transformation of CVR data is clinically useful; such issues should certainly be addressed going forward. We also anticipate that different neurologic diseases may call for different stimulus patterns and their respective normal atlases, to reveal their pathophysiology. Certain patterns (square wave, sinusoidal, ramp, pulse, and others) may be optimum to study certain conditions (vasculitis, traumatic brain injury, subarachnoid hemorrhage, and others). The overarching approach nevertheless would be the same: score patient CVR datasets with respect to a relevant reference atlas.

Blood pressure is a key confounding factor, which effects the interpretation of CVR.[43] However, in these experiments we were limited by the constraints the MRI environment imposes on blood pressure measurement.

SUMMARY AND CONCLUSION

In this paper we describe a secondary analysis of CVR maps consisting of a voxel-by-voxel scoring of CVR maps about a reference atlas leading to a quantitative approach to the assessment of pathologic CVR. In the example analyses of individual subject CVR maps in patients with known steno-occlusive diseases of the cervico-cerebral vasculature, the *z*-map assessment appeared to enhance the resolution of the presence, localization, and severity of pathologic CVR. We therefore concluded that the *z*-map scoring and analysis of CVR studies has the potential to reduce the confounding effects of test-to-test, subject-to-subject, and platform-to-platform variability for comparison of CVR studies.

DISCLOSURE/CONFLICT OF INTEREST

JAF is the Chief Scientist and JD is the Senior Scientist at Thornhill Research (TRI), a spin-off company from the University Health Network that developed the RespirAct™. RespirAct™ is currently a noncommercial research tool assembled, and made available by TRI to research institutions to enable CVR studies.

ACKNOWLEDGMENTS

The authors thank the Toronto Western Hospital MRI technologists, in particular Eugen Hlasny and Keith Ta for their help in acquiring the data.

REFERENCES

1 Sobczyk O, Battisti-Charbonney A, Fierstra J, Mandell DM, Poublanc J, Crawley AP *et al.* A conceptual model for CO2-induced redistribution of cerebral blood flow with experimental confirmation using BOLD MRI. *Neuroimage* 2014; **92**: 56–68.
2 Fierstra J, Poublanc J, Han JS, Silver F, Tymianski M, Crawley AP *et al.* Steal physiology is spatially associated with cortical thinning. *J Neurol Neurosurg Psychiatry* 2010; **81**: 290–293.
3 Mandell DM, Han JS, Poublanc J, Crawley AP, Kassner A, Fisher JA *et al.* Selective reduction of blood flow to white matter during hypercapnia corresponds with leukoaraiosis. *Stroke* 2008; **39**: 1993–1998.
4 Han JS, Mikulis DJ, Mardimae A, Kassner A, Poublanc J, Crawley AP *et al.* Measurement of cerebrovascular reactivity in pediatric patients with cerebral vasculopathy using blood oxygen level-dependent MRI. *Stroke* 2011; **42**: 1261–1269.
5 Fierstra J, Conklin J, Krings T, Slessarev M, Han JS, Fisher JA *et al.* Impaired peri-nidal cerebrovascular reserve in seizure patients with brain arteriovenous malformations. *Brain* 2011; **134**: 100–109.
6 Han JS, Mandell DM, Poublanc J, Mardimae A, Slessarev M, Jaigobin C *et al.* BOLD-MRI cerebrovascular reactivity findings in cocaine-induced cerebral vasculitis. *Nat Clin Pract Neurol* 2008; **4**: 628–632.
7 Conklin J, Fierstra J, Crawley AP, Han JS, Poublanc J, Mandell DM *et al.* Impaired cerebrovascular reactivity with steal phenomenon is associated with increased diffusion in white matter of patients with Moyamoya disease. *Stroke* 2010; **41**: 1610–1616.
8 Balucani C, Viticchi G, Falsetti L, Silvestrini M. Cerebral hemodynamics and cognitive performance in bilateral asymptomatic carotid stenosis. *Neurology* 2012; **79**: 1788–1795.
9 Silvestrini M, Viticchi G, Falsetti L, Balucani C, Vernieri F, Cerqua R *et al.* The role of carotid atherosclerosis in Alzheimer's disease progression. *J Alzheimers Dis* 2011; **25**: 719–726.
10 Silvestrini M, Vernieri F, Pasqualetti P, Matteis M, Passarelli F, Troisi E *et al.* Impaired cerebral vasoreactivity and risk of stroke in patients with asymptomatic carotid artery stenosis. *JAMA* 2000; **283**: 2122–2127.
11 Markus H, Cullinane M. Severely impaired cerebrovascular reactivity predicts stroke and TIA risk in patients with carotid artery stenosis and occlusion. *Brain* 2001; **124**: 457–467.
12 Ito H, Kanno I, Ibaraki M, Hatazawa J. Effect of aging on cerebral vascular response to Paco2 changes in humans as measured by positron emission tomography. *J Cereb Blood Flow Metab* 2002; **22**: 997–1003.
13 Kastrup A, Thomas C, Hartmann C, Schabet M. Sex dependency of cerebrovascular CO2 reactivity in normal subjects. *Stroke* 1997; **28**: 2353–2356.
14 Spano VR, Mandell DM, Poublanc J, Sam K, Battisti-Charbonney A, Pucci O *et al.* CO2 blood oxygen level-dependent MR mapping of cerebrovascular reserve in a clinical population: safety, tolerability, and technical feasibility. *Radiology* 2013; **266**: 592–598.
15 Fierstra J, Sobczyk O, Battisti-Charbonney A, Mandell DM, Poublanc J, Crawley AP *et al.* Measuring cerebrovascular reactivity: what stimulus to use?. *J Physiol* 2013; **591**: 5809–5821.
16 Somogyi RB, Vesely AE, Preiss D, Prisman E, Volgyesi G, Azami T *et al.* Precise control of end-tidal carbon dioxide levels using sequential rebreathing circuits. *Anaesth Intensive Care* 2005; **33**: 726–732.
17 Slessarev M, Han J, Mardimae A, Prisman E, Preiss D, Volgyesi G *et al.* Prospective targeting and control of end-tidal CO2 and O2 concentrations. *J Physiol* 2007; **581**: 1207–1219.
18 Ito S, Mardimae A, Han J, Duffin J, Wells G, Fedorko L *et al.* Non-invasive prospective targeting of arterial PCO2 in subjects at rest. *J Physiol* 2008; **586**: 3675–3682.
19 Willie CK, Macleod DB, Shaw AD, Smith KJ, Tzeng YC, Eves ND *et al.* Regional brain blood flow in man during acute changes in arterial blood gases. *J Physiol* 2012; **590**: 3261–3275.
20 Cox RW. AFNI: software for analysis and visualization of functional magnetic resonance neuroimages. *Comput Biomed Res* 1996; **29**: 162–173.
21 Saad ZS, Glen DR, Chen G, Beauchamp MS, Desai R, Cox RW. A new method for improving functional-to-structural MRI alignment using local Pearson correlation. *Neuroimage* 2009; **44**: 839–848.
22 Ashburner J, Friston KJ. Nonlinear spatial normalization using basis functions. *Hum Brain Mapp* 1999; **7**: 254–266.
23 Ashburner J, Friston K. Multimodal image coregistration and partitioning—a unified framework. *Neuroimage* 1997; **6**: 209–217.
24 Minoshima S, Frey KA, Koeppe RA, Foster NL, Kuhl DE. A diagnostic approach in Alzheimer's disease using three-dimensional stereotactic surface projections of fluorine-18-FDG PET. *J Nucl Med* 1995; **36**: 1238–1248.
25 Houston AS, Kemp PM, Macleod MA. A method for assessing the significance of abnormalities in HMPO brain SPECT images. *J Nucl Med* 1994; **35**: 239–244.
26 Seitz RJ, Bohm C, Greitz T, Roland PE, Eriksson L, Blomqvist G *et al.* Accuracy and precision of the computerized brain atlas programme for localization and quantification in positron emission tomography. *J Cereb Blood Flow Metab* 1990; **10**: 443–457.
27 Totaro R, Marini C, Baldassarre M, Carolei A. Cerebrovascular reactivity evaluated by transcranial Doppler: reproducibility of different methods. *Cerebrovasc Dis* 1999; **9**: 142–145.
28 Mark CI, Fisher JA, Pike GB. Improved fMRI calibration: precisely controlled hyperoxic versus hypercapnic stimuli. *Neuroimage* 2011; **54**: 1102–1111.
29 Baddeley H, Brodrick PM, Taylor NJ, Abdelatti MO, Jordan LC, Vasudevan AS *et al.* Gas exchange parameters in radiotherapy patients during breathing of 2%, 3.5% and 5% carbogen gas mixtures. *Br J Radiol* 2000; **73**: 1100–1104.
30 Fierstra J, Winter J, Machina M, Lukovic J, Duffin J, Kassner A *et al.* Non-invasive accurate measurement of arterial PCO2 in a pediatric animal model. *J Clin Monit Comput* 2013; **27**: 147–155.
31 Chetelat G, Desgranges B, Landeau B, Mezenge F, Poline JB, de la Sayette V *et al.* Direct voxel-based comparison between grey matter hypometabolism and atrophy in Alzheimer's disease. *Brain* 2008; **131**: 60–71.
32 Ishii K, Sasaki M, Matsui M, Sakamoto S, Yamaji S, Hayashi N *et al.* A diagnostic method for suspected Alzheimer's disease using H(2)15O positron emission tomography perfusion Z score. *Neuroradiology* 2000; **42**: 787–794.
33 Commowick O, Fillard P, Clatz O, Warfield SK. Detection of DTI white matter abnormalities in multiple sclerosis patients. *Med Image Comput Comput Assist Interv* 2008; **11**: 975–982.
34 Kemp PM, Houston AS, Macleod MA, Pethybridge RJ. Cerebral perfusion and psychometric testing in military amateur boxers and controls. *J Neurol Neurosurg Psychiatry* 1995; **59**: 368–374.
35 Takahashi N, Lee Y, Tsai DY, Kinoshita T, Ouchi N, Ishii K. Computer-aided detection scheme for identification of hypoattenuation of acute stroke in unenhanced CT. *Radiol Phys Technol* 2012; **5**: 98–104.
36 Takahashi N, Tsai DY, Lee Y, Kinoshita T, Ishii K, Tamura H *et al.* Usefulness of z-score mapping for quantification of extent of hypoattenuation regions of hyperacute stroke in unenhanced computed tomography: analysis of radiologists' performance. *J Comput Assist Tomogr* 2010; **34**: 751–756.
37 Hoge RD, Atkinson J, Gill B, Crelier GR, Marrett S, Pike GB. Investigation of BOLD signal dependence on cerebral blood flow and oxygen consumption: the deoxyhemoglobin dilution model. *Magn Reson Med* 1999; **42**: 849–863.
38 Arbab AS, Aoki S, Toyama K, Miyazawa N, Kumagai H, Umeda T *et al.* Quantitative measurement of regional cerebral blood flow with flow-sensitive alternating inversion recovery imaging: comparison with [iodine 123]-iodoamphetamin single photon emission CT. *AJNR Am J Neuroradiol* 2002; **23**: 381–388.
39 Mandell DM, Han JS, Poublanc J, Crawley AP, Stainsby JA, Fisher JA *et al.* Mapping cerebrovascular reactivity using blood oxygen level-dependent MRI in patients with arterial steno-occlusive disease: comparison with arterial spin labeling MRI. *Stroke* 2008; **39**: 2021–2028.
40 Galvin SD, Celi LA, Thomas KN, Clendon TR, Galvin IF, Bunton RW *et al.* Effects of age and coronary artery disease on cerebrovascular reactivity to carbon dioxide in humans. *Anaesth Intensive Care* 2010; **38**: 710–717.
41 Schwertfeger N, Neu P, Schlattmann P, Lemke H, Heuser I, Bajbouj M. Cerebrovascular reactivity over time course in healthy subjects. *J Neurol Sci* 2006; **249**: 135–139.
42 Oudegeest-Sander MH, van Beek AHEA, Abbink K, Olde Rikkert MGM, Hopman MTE, Claassen JAHR. Assessment of dynamic cerebral autoregulation and cerebrovascular CO2 reactivity in aging by measurements of cerebral blood flow and cortical oxygenation. *Exp Physiol* 2013; **99**: 586–598.
43 Regan RE, Fisher JA, Duffin J. Factors affecting the determination of cerebrovascular reactivity. *Brain Behav* 2014; **4**: 775–788.
44 Sam K, Small E, Poublanc J, Han JS, Mandell DM, Fisher JA *et al.* Reduced contralateral cerebrovascular reserve in patients with unilateral steno-occlusive disease. *Cerebrovasc Dis* 2014; **38**: 94–100.